Tunneling through rectangular quantum dots at high magnetic fields

Zhen-Li Ji

Department of Physics and Measurement Technology, Linköping University, S-581 83 Linköping, Sweden

Transport in a quasi-one-dimensional wire containing a rectangular quantum dot in a strong magnetic field is studied numerically. As the width of the wire is varied, a rectangular dot on the wire introduces peak or dip structures in the conductance. The charge-density distribution and current-flow pattern clearly show that the Landau-level coupling between the zero-dimensional (0D) state and the extended state is the origin of these structures. At the resonant points, which correspond to 0D states in the dot, Landau-level coupling becomes essential and the propagation of one Landau level is enhanced or blocked by the 0D state of a different Landau level.

I. INTRODUCTION

Magnetotransport along edge states that are formed in a high-mobility two-dimensional electron gas (2DEG) is currently a subject of great experimental and theoretical interest.[1] Recently, quasi-zero-dimensional systems have received considerable attention. Transport through semiconductor quantum dots shows striking effects due to the electron wave nature and its finite charge. Experiments are now done on quantum dots where Coulomb interactions, zero-dimensional (0D) states, and edge states exist.[2-16] Such experiments have encouraged theoretical efforts analyzing some fundamental phenomena such as Coulomb blockade in resonant tunneling, and Aharonov-Bohm or fractional quantum Hall effects.[17-28] In particular, physical insight has been gained by establishing a connection between resonances (antiresonances) of the open system on the one hand, and bound states on the other, typically belonging to some closely related isolated system.[10-16]

The discrete spectrum of dots, which has been explored by various spectroscopic techniques, causes such transport effects as Coulomb blockade and resonant tunneling.[2-9] A peak (dip) in the conductance of the dot due to resonance (antiresonance) should be seen when an electron state of the dot lines up with the Fermi energy in the leads. Although many resonant and antiresonant peaks have been observed in these structures, the nature of these resonances has not been clearly understood. Some fundamental phenomena, such as the Coulomb blockade, the Aharonov-Bohm effect, and the fractional quantum Hall effect, have attracted significant attention recently. However, existing theories do not address the effects of the Landau-level (LL) coupling in magnetotunneling through semiconductor quantum dots. For magnetotransport along edge states, the LL coupling in different regions of the device is essential in tunneling processes. The purpose of this paper is to present a numerical study of rectangular quantum dots at high magnetic fields, where 0D state influence is significant for the magnetotransport. The system that we will treat here has also been realized in practice.[29] It consists of a wire

in which a rectangular box is defined by two transverse gate barriers. Recently Palacios *et al.*[26] have studied the Coulomb-blockade and Aharonov-Bohm effects in a similar system. However, we will focus on the influence of 0D states on magnetotransport. We show that a peak (or a dip) in the conductance is due to the coupling between the LL in the leads and a 0D state belonging to one of the Landau levels (LL's) in the dot when the energy of a 0D state in the dot coincides with the Fermi energy. The conductance is well quantized when the Fermi energy in the leads does not line up with the 0D state in the dot. The calculation is performed in the framework of a one-electron Schrödinger model, neglecting electron-electron interactions. We believe, however, that the LL coupling between the dot and leads is essential for transport at high magnetic fields; electron-electron interactions are unlikely to alter the qualitative fact of the presence of LL coupling in magnetotransport.

The outline of this paper is as follows. In Sec. II we present the model and theoretical formulation. Section III presents numerical results. In particular, it is shown that the 0D states in the dot give rise to peaks and dips in the conductance. These peaks (dips) are associated with resonant (antiresonant) tunneling. The final section contains some concluding remarks.

II. THEORY

In this section we will present the theoretical method we use to compute the magnetoconductance of a dot attached to two leads. The mode-matching method is used in this problem. In principle the formalism we discuss here is elementary, but we prefer to present it for completeness and believe that it may be useful.

The quantum wire considered here has infinite length in the x direction and is confined in the region $-W/2 < y < W/2$ by hard walls in the y direction. In Fig. 1 such a quantum wire is shown, including two square potential barriers each of length d and height $V = V_b$. A quantum box is defined by means of two barriers crossing the wire of width W separated by a distance L in
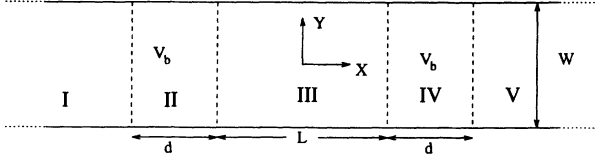
FIG. 1. Schematic diagram of a rectangular dot in an electron waveguide. The electrons are confined between the two horizontal lines and experience a barrierlike potential in the regions marked $V = V_b$. The potential elsewhere is zero. The regions I–V are used in the expansion of wave functions that are to be matched across the boundaries represented by the dashed lines.

$V = 0$. The system consists of five regions as shown in Fig. 1. The regions I–V are used in the expansion of wave functions that are to be matched across the boundaries represented by the dashed lines.

The Schrödinger equation describing electrons in this structure is

$$\frac{(\mathbf{P} + e\mathbf{A})^2}{2m^*} \psi(x,y) + V(y)\psi(x,y) = (E - V)\psi(x,y) ,$$

$$V(y) = \begin{cases} 0, & |y| < W/2 \\ \infty, & |y| \geq W/2, \end{cases} \tag{1}$$

where m^* is the effective mass and $\mathbf{A}$ is the vector potential. The magnetic field is directed along the z direction. We choose the Landau gauge

$$\mathbf{A} = (-By, 0, 0) , \tag{2}$$

where B is the magnetic flux density. Thus Eq. (1) may be solved in the separable form[30]

$$\psi^{\pm}(x,y) = e^{\pm ik_x x}\Phi^{\pm}(y) , \tag{3}$$

where k_x is the x-directed wave vector and $\Phi^{\pm}(y)$ satisfies the equation

$$\frac{d^2\Phi^{\pm}(y)}{dy^2} + k^2\Phi^{\pm}(y) - \left(\frac{y}{l^2} \mp k_x\right)^2 \Phi^{\pm}(y) = 0 . \tag{4}$$

Here l is the magnetic length defined by $l^2 = \hbar/eB$, and $k^2 = 2m^*(E - V)/\hbar^2$. For a given energy $(E = E_F)$ and magnetic field B we obtain three kinds of modes,[27,31] the propagating mode whose wave number is real, the oscillatory damped mode whose wave number is complex, and the evanescent mode whose wave number is purely imaginary. If we turn off the magnetic field completely, wave number k_x is either purely real or purely imaginary, corresponding to parabolic dispersion relations of subbands below or above the chosen energy, respectively.

To find the wave functions $\Phi^{\pm}(y)$ of the magnetoelectric states, we have to solve Eq. (4) subject to the boundary conditions

$$\Phi^{\pm}(y = -W/2) = \Phi^{\pm}(y = W/2) = 0 . \tag{5}$$

For nonzero B the $\Phi^{\pm}(y)$ are each a combination of Kummer functions and are not orthogonal. The properties of the functions $\Phi^{\pm}(y)$ can be found in Ref. 31.

We will, however, choose an expansion method. Thus we obtain the eigenvalues k_x and the functions $\Phi^{\pm}(y)$ in the following way. The wave functions $\Phi^{\pm}(y)$ are expanded by an orthonormal set of the N eigenstates ϕ_m's of the reduced Hamiltonian for $B = 0$ with expansion coefficients $a_m^{\pm}$,

$$\Phi^{\pm}(y) = \sum_{m=1}^{N} a_m^{\pm}\phi_m(y) , \tag{6}$$

where $\phi_m(y) = (2/W)^{1/2}\sin\left[\frac{m\pi}{W}\left(y + \frac{W}{2}\right)\right]$. Substituting Eq. (6) into Eq. (4), multiplying by $\phi_j(y)$, and integrating from $-W/2$ to $W/2$, we obtain

$$\sum_{m=1}^{N}\left\{\left[k^2 - \left(\frac{j\pi}{W}\right)^2\right]\delta_{jm} - \langle j|\left[\frac{y}{l^2} \mp k_x\right]^2|m\rangle\right\}c_m = 0 , \tag{7}$$

where

$$\langle j|y|m\rangle = \frac{2}{W}\int_{-W/2}^{W/2} dy\, y \sin\left[\frac{j\pi}{W}\left(y + \frac{W}{2}\right)\right]$$
$$\times \sin\left[\frac{m\pi}{W}\left(y + \frac{W}{2}\right)\right] .$$

The problem now is to find k_x. We do that by using the following trick.[30] Let $c_m = k_x a_m$. Equation (7) can now be recast as

$$\begin{pmatrix} \mathbf{0} & \mathbf{1} \\ \mathbf{S} & \mathbf{T} \end{pmatrix}\begin{pmatrix} \mathbf{a} \\ \mathbf{c} \end{pmatrix} = k_x\begin{pmatrix} \mathbf{a} \\ \mathbf{c} \end{pmatrix}, \tag{8}$$

with

$$(\mathbf{S})_{jm} = \left[k^2 - \left(\frac{j\pi}{W}\right)^2\right]\delta_{jm} - \frac{1}{l^4}\langle j|y^2|m\rangle ,$$

$$(\mathbf{T})_{jm} = \frac{2}{l^2}\langle j|y|m\rangle . \tag{9}$$

Solving Eq. (8) we obtain $2N$ eigenvalues $\left(\pm k_x^1, \pm k_x^2, \ldots, \pm k_x^N\right)$ for any given energy E and find the corresponding eigenvectors which give the wave functions $\Phi_n^{\pm}(y)$. Each value of n corresponds to a magnetoelectric subband.

For an electron injected from the left into the nth mode, the incident and reflecting modes must be taken into account, and one has

$$\Psi_n^{\mathrm{I}}(x,y) = e^{ik_x^n x}\Phi_n^{+}(y) + \sum_m B_{nm}^{\mathrm{I}}e^{-ik_x^m x}\Phi_m^{-}(y) , \tag{10}$$

where the coefficients B_{nm}^{I} give the probability amplitudes for reflection, and k_x^i may be real, complex, or purely imaginary.[27] Similarly, the wave function in region V is given by a sum of outgoing modes, i.e.,

$$\Psi_n^{\mathrm{V}}(x,y) = \sum_m C_{nm}^{\mathrm{V}}e^{ik_x^m x}\Phi_m^{+}(y) , \tag{11}$$

where C_{nm}^{V} gives the transmission probability. In regions

II, III, and IV, there are no restrictions and all the solutions must be taken into account. So the solution looks like this:

$$\Psi_n^K (x,y) = \sum_m \left[B_{nm}^K e^{-ik_x^m x} \Phi_m^- (y) + C_{nm}^K e^{ik_x^m x} \Phi_m^+ (y) \right],$$
(12)

where K =II, III, and IV, and B_{nm}^K and C_{nm}^K are expansion coefficients which depend on the incident wave.

Now matching the wave function and its normal derivative at every boundary in a procedure similar to that reported previously[32] leads to an infinite set of linear equations for the expansion coefficients. This infinite set of equations is solved numerically using a truncation procedure, keeping a finite number of modes, large enough to achieve a desired convergence or accuracy. We check numerical convergence by how well unitarity at the dot is obeyed. The relationship should be $\sum_m (T_{nm} + R_{nm}) = 1$, where T_{nm} is the transmission from incident mode n to final mode m and R_{nm} is the reflection. Typically, one has to include all the subbands below Fermi energy E_F, the subbands above that energy with complex wave numbers, and several subbands with purely imaginary wave numbers.[27] For the results presented in this paper, we use 12 transverse modes, and see unitarity violated in the fourth decimal place. With these expansion coefficients at hand we can easily evaluate the transmission probability, charge-density distribution, and current distribution. For propagating modes n and m the transmission from mode n in region I to mode m in region V is given by

$$T_{nm} = \frac{v_m}{v_n} \left| C_{nm}^{\mathrm{V}} \right|^2 ,$$
(13)

where v_i is the velocity in the x direction of the ith mode in region I or V and is defined as

$$v_i = \frac{\hbar}{m^*} \int dy \Phi_i^{+*} (y) \left[k_x^i - \frac{eB}{\hbar} y \right] \Phi_i^+ (y) .$$
(14)

The linear-response conductance of the system is calculated from the Landauer-Büttiker formula

$$G = \frac{2e^2}{h} \sum_{n,m=1}^M T_{nm} ,$$
(15)

where M is the number of propagating modes in region I or V.

In linear-response transport at low temperatures, only electrons at the Fermi level carry a net current. The two-dimensional electron current density $\mathbf{j}_m (x,y)$ of the mth mode is calculated directly from the wave function $\Psi_m (x,y)$ of electrons in that mode through the relation

$$\mathbf{j}_m (x,y) = -\frac{\hbar}{m^*} \mathrm{Im} \left[\Psi_m (x,y) \nabla \Psi_m^* (x,y) \right]$$
$$+ \frac{e}{m^*} \mathbf{A} \left| \Psi_m (x,y) \right|^2 .$$
(16)

The total current density at the Fermi energy is calculated by vectorially adding the contributions from all propagating states

$$\mathbf{J} (x,y) = \sum_{m=1}^M \mathbf{j}_m (x,y) /v_m .$$
(17)

Note that the contribution of each propagating mode to the total current density is weighted by the corresponding group velocity so that each mode at the Fermi energy carries a unit flux. The probability density is given by[33]

$$\rho (x,y) = \sum_{m=1}^M \left| \Psi_m (x,y) \right|^2 /v_m .$$
(18)

In the following, we will assume an effective mass $m^* = 0.067 m_0$, which is appropriate for the $\mathrm{Al}_x \mathrm{Ga}_{1-x} \mathrm{As}/\mathrm{GaAs}$ interface.

III. NUMERICAL RESULTS

In Figs. 2(a) and 2(b), we show the conductance G as a function of the channel width W for two different values of the dot length L. The height of the barriers is 2 meV and the width of them 80 nm (we restrict ourselves here to the symmetrical case of equal barriers). The Fermi energy is 6 meV and two LL's are occupied at $B = 2$ T. The first LL has enough kinetic energy to overcome the barriers, but the second one cannot. A series of periodic dips is observed in the conductance profile in addition to the well-known conductance quantization. For large values of L, the distance between two dips becomes short. We now discuss the origin of this behavior. The periodicity of the series of conductance dips shown in Figs. 2(a) and 2(b) can be understood by the LL coupling between the 0D state and the extended state. To un-
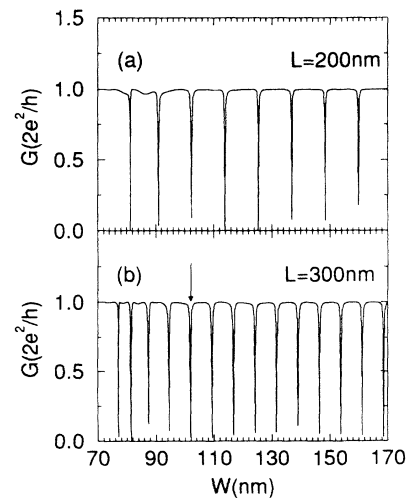

FIG. 2. Conductance as a function of the width W for the structure with $V_b = 2$ meV, $d = 80$ nm, $B = 2$ T, and $E = 6$ meV. (a) and (b) refer to $L = 200$ nm and 300 nm, respectively. The arrow indicates the width W corresponding to the charge-density distribution shown in Fig. 4(b).

derstand why the conductance G exhibits periodic dips, energy spectra of an electron system confined in a rectangular box with infinite walls are shown in Fig. 3. The condensation of the 0D states of the dot into degenerate LL's is clearly evident in the figure. In the parameter range we are concerned with, the spectrum consists of two sets of LL's, which are composed of discrete nondegenerate states because of the confinement potential. The horizontal line at 6 meV in Fig. 3 indicates the Fermi energy which corresponds to the value used in Figs. 2(a) and 2(b). The electron alternately occupies a 0D state in the first LL and a state in the second LL as the width of the wire is increased. When the electron state of the dot in the second LL lines up with the Fermi energy in the leads, a dip in the conductance of the dot due to antiresonance can be seen in Figs. 2(a) and 2(b). The overlap between electron wave functions belonging to the second LL in the dot and the first LL in the leads, respectively, is minimal. Figures 4(a) and 4(b) show the charge-density distributions in a rectangular box with infinite walls at a bound state belonging to the second LL ($W_y = 109.3$ nm, denoted by an arrow in Fig. 3) and in a quantum box built up on a quantum wire by means of two finite barriers at a conductance dip [$W = 102$ nm, denoted by an arrow in Fig. 2(b)], respectively. The electron-density distribution of Fig. 4(b) is qualitatively very similar to that of an isolated dot shown in Fig. 4(a). We also found this kind of similarity for other cases. Therefore the dip structure in Figs. 2(a) and 2(b) is found to originate from complete backscattering through 0D states of the dot in the second LL. On the other hand, when a 0D state of the dot in the first LL lines up with the Fermi energy in the leads, the first LL in the leads tunnels through
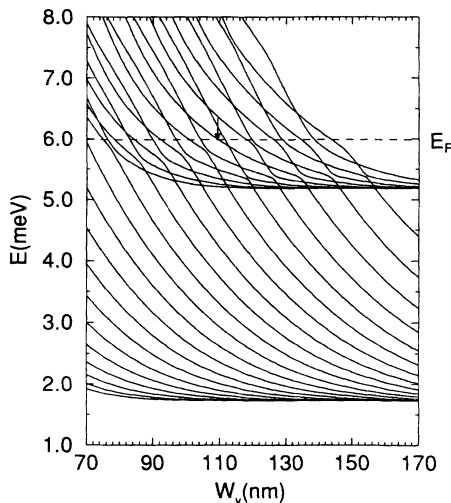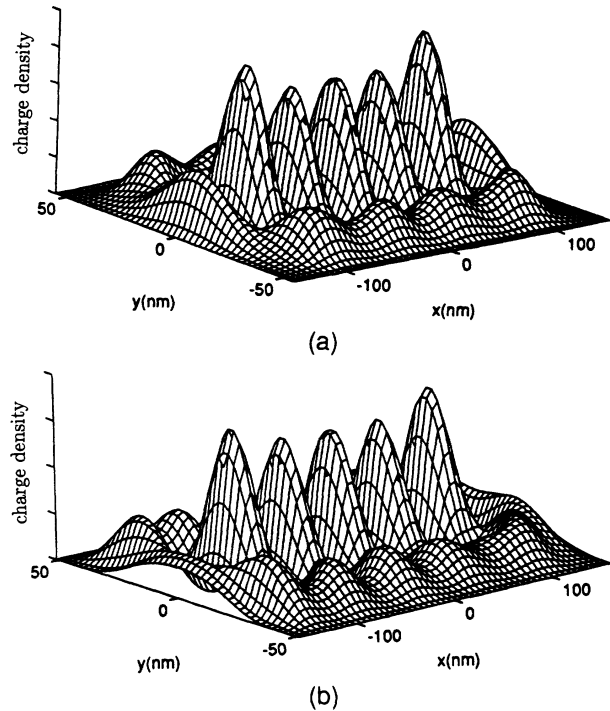

(a)

(b)

FIG. 4. (a) The charge-density distribution of a rectangular dot with infinite walls in the state that is 22nd lowest in energy. $W_y = 109.3$ nm, denoted by an arrow in Fig. 3. (b) The charge-density distribution of the structure shown in Fig. 1. $W = 102$ nm, denoted by an arrow in Fig. 2(b).

FIG. 3. Energy levels of a rectangular dot with infinite walls as a function of y-directed width W_y in a parameter range where two LL's are present. The magnetic field is $B = 2$ T and the x-directed width is $W_x = 300$ nm. The horizontal line at 6 meV indicates the Fermi energy. [These numerical values correspond to the calculation in Fig. 2(b).] The arrow indicates the case corresponding to the charge-density distribution shown in Fig. 4(a).

the dot coherently, with no effect on the conductance in Figs. 2(a) and 2(b). At a particular W, the 0D state of the dot lines up with the Fermi energy in the leads. There are two possible couplings between the 0D state in the dot and a propagating LL in the leads. If the 0D state of the dot is in the first LL, it couples well to the first LL in the leads and transport can occur by coherent tunneling through this state, that is, the transmission is 1, and there is no effect on the conductance. If the 0D state of the dot is in the second LL, however, the conductance is suppressed since the coupling to this state is minimal. A dip in conductance is thus expected whenever the 0D state of the dot belongs to the second LL.

Figure 5 presents the conductance as a function of the width W for the values of $B = 2$ T, $V_b = 3$ meV, $E_F = 8$ meV, and $L = 150$ nm. There clearly appear three different regions (hereafter labeled as region A, region B, and region C, respectively). Region A corresponds to the case of having only one LL occupied in the leads and dot with the kinetic energy of the edge state not high enough for the electron to pass over the barriers. The peaks in the conductance correspond to resonant tunneling through quasibound states in the dot. Coulomb effects play an important role in the quasi-one-dimensional transport between two leads in region A since the number of electrons confined in the dot is a well-defined quantity and corresponds to an integer number. It is beyond the scope of the present model study to include Coulomb effects. Palacios et al.[26] have examined the influence of
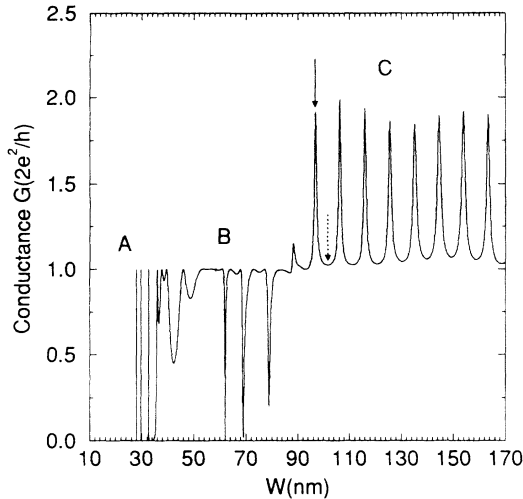
FIG. 5. Conductance vs width W for a Fermi energy of 8 meV in a magnetic field of 2 T. The length L of the box is 150 nm. The height of the barriers is 3 meV and the width d of them 80 nm. The arrows indicate the width W corresponding to the charge-density distributions and current distributions shown in Figs. 6(a)–6(d).

Coulomb interaction on the conductance of a similar system, and show that the actual conductance up to six electrons is essentially the single-particle transmission shifted and broadened by charging effects. In region B of Fig. 5 two LL's are occupied in the leads and dot, which is similar to the cases in Figs. 2(a) and 2(b). A few narrow dips are observed in the conductance in addition to the steplike structure due to the first LL running free over the barriers. The dips occur if the 0D state of the second LL in the dot lines up with the Fermi energy in the leads.

Let us now turn our attention to region C of Fig. 5 in which two LL's are occupied. The first one has enough

kinetic energy to overcome the barrier freely, and the second one has a kinetic energy of the edge state high enough for the electron to tunnel through the dot via the 0D state. There is a series of nearly periodic peaks in the conductance as a function of W. The origin of these peak structures can be considered as resonant tunneling through 0D states belonging to the second LL. If the 0D state of the dot is in the second LL, it couples well to the second LL in the leads. The second LL starts to propagate by resonant tunneling through this state, resulting in a resonant peak. When the energy of the incident electron takes the value corresponding to the energy of the 0D state of the first LL existing in the dot, the electron of the second LL in the leads is perfectly reflected by the dot, since there exists no coupling between the first LL and the second LL. As a result, the number of LL's contributing to the conductance is 1.

Having understood the behavior of conductance peaks and dips, we now pay attention to the behavior of the charge-density distributions and current distributions in the system. In Figs. 6(a) and 6(b), we have plotted the charge-density distribution and current distribution, respectively, for a conductance peak ($W = 96.9$ nm, denoted by a solid arrow in Fig. 5). The current-flow pattern at the peak shows that there is no edge state along the perimeter of the dot. As expected, in the case of resonant tunneling, the charge-density distribution and current distribution clearly show that 0D states have formed and the bulk of the current circulates in the dot. In Figs. 6(c) and 6(d), we show the charge-density distribution and current distribution for the case that the first LL has enough kinetic energy to overcome the barriers, but the second one is perfectly reflected ($W = 101.5$ nm, denoted by a dotted arrow also in Fig. 5). The charge density piles up near an edge because of the Lorentz force skewing the wave function towards that edge. The current pattern in Fig. 6(d) shows that edge states have
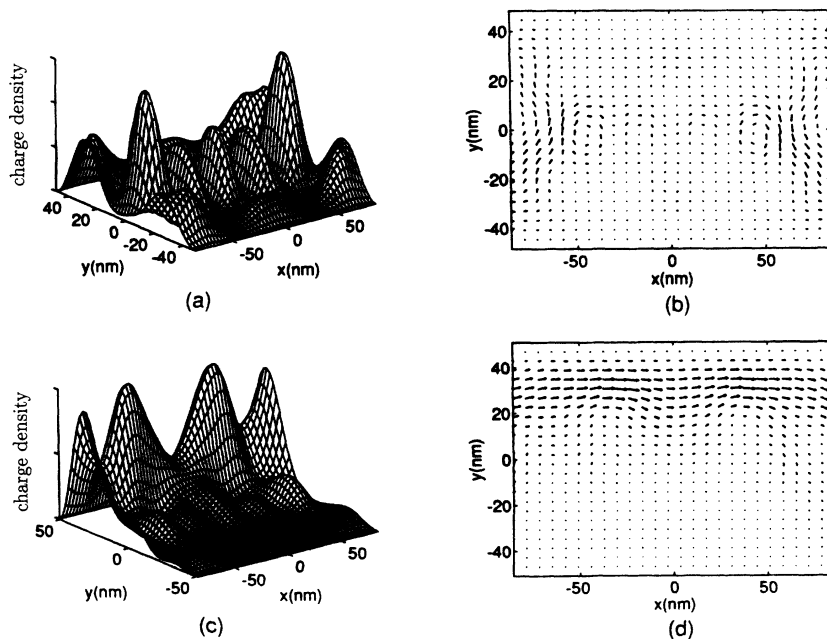

(a)

(b)

(c)

(d)

FIG. 6. The spatial distributions for the cases denoted by the arrows in Fig. 5. (a) The charge-density distribution associated with the resonant tunneling via a 0D state at $W = 96.9$ nm, denoted by a solid arrow in Fig. 5. (b) The current distribution associated with the charge-density distribution in (a). (c) The charge-density distribution at $W = 101.5$ nm, denoted by a dotted arrow also in Fig. 5. (d) The current distribution associated with the charge-density distribution in (c). The bulk of the forward current is carried by edge states.

formed and carry the bulk of the forward current. This picture is repeated periodically as the width of the quantum wire is swept.

IV. CONCLUDING REMARKS

In this paper, we have investigated lateral magnetotunneling through rectangular quantum dots. The conductance, charge-density distributions, and current distributions were calculated. We have shown that the propagation of one LL is enhanced or blocked by the 0D state of different LL's in the dot, resulting in the appearance of resonant peaks or antiresonant dips in conductance. The charge-density distributions and current-flow patterns clearly show that LL coupling between the 0D state and the extended state is the origin of these peaks and dips. We propose that recent experimental measurements may be interpreted in these terms.[10,13,16,29] We recall that the calculations here are based on a very idealized model potential. In reality, the potential barrier in a semiconductor structure will not be a perfect step function. However, smooth deviations in the shape of the potential from that of a square barrier do not lead to important changes in the conductance.[34] In this one-electron Schrödinger model Coulomb effects have been neglected. The Coulomb interaction has important implications in weakly conducting regimes (conductance $G < e^2/h$). The energy-level spectrum of a dot in a high magnetic field can be affected by electron-electron interactions.[11,18] This could have influence on the structure of the dips and peaks in the conductance. An improved theory would include Coulomb effects to account for the accumulation of charge in the dot. Because the coupling between the dot and leads is essential for the transport and LL's have formed in the cases we discussed here, such an improvement is unlikely to alter the basic results.

ACKNOWLEDGMENTS

[1] C. W. J. Beenakker and H. van Houten, in *Solid State Physics: Advances in Research and Applications*, edited by H. Ehrenreich and D. Turnbull (Academic, New York, 1991), Vol. 44, p. 1, and references cited therein.

[2] T. P. Smith III, K. Y. Lee, C. M. Knoedler, J. M. Hong, and D. P. Kern, Phys. Rev. B **38**, 2172 (1988).

[3] W. Hansen, T. P. Smith III, K. Y. Lee, J. A. Brum, C. M. Knoedler, J. M. Hong, and D. P. Kern, Phys. Rev. Lett. **62**, 2168 (1989).

[4] Ch. Sikorski and U. Merkt, Phys. Rev. Lett. **62**, 2164 (1989).

[5] M. A. Reed, J. N. Randall, R. J. Aggarwal, R. J. Matyi, T. M. Moore, and A. E. Wetsel, Phys. Rev. Lett. **60**, 535 (1988).

[6] B. J. van Wees, L. P. Kouwenhoven, C. J. P. M. Harmans, J. G. Williamson, C. E. Timmering, M. E. I. Broekaart, C. T. Foxon, and J. J. Harris, Phys. Rev. Lett. **62**, 2523 (1989).

[7] B. J. van Wees *et al.*, Phys. Rev. B **39**, 8066 (1989).

[8] C. Pasquier, U. Mertav, F. I. B Williams, D. C. Glattli, Y. Jin, and B. Etienne, Phys. Rev. Lett. **70**, 69 (1993).

[9] U. Meirav, M. A. Kastner, H. Heiblum, and S. J. Wind, Phys. Rev. Lett. **65**, 771 (1990).

[10] P. L. McEuen, E. B. Foxman, U. Meirav, M. A. Kastner, Yigal Meir, Ned S. Wingreen, and S. J. Wind, Phys. Rev. Lett. **66**, 1926 (1991).

[11] P. L. McEuen, E. B. Foxman, J. Kinaret, U. Meirav, M. A. Kastner, N. S. Wingreen, and S. J. Wind, Phys. Rev. B **45**, 11 419 (1992).

[12] A. S. Sachrajda, R. P. Taylor, C. Dharma-Wardana, P. Zawadzki, J. A. Adams, and P. T. Coleridge, Phys. Rev. B **47**, 6811 (1993).

[13] B. W. Alphenaar, A. A. M. Staring, H. van Houten, M. A. A. Mabesoone, O. J. A. Buyk, and C. T. Foxon, Phys. Rev. B **46**, 7236 (1992).

[14] A. T. Johnson, L. P. Kouwenhoven, W. de Jong, N. C. van der Vaart, C. J. P. M. Harmans, and C. T. Foxon, Phys. Rev. Lett. **69**, 1592 (1992).

[15] B. Meurer, D. Heitmann, and K. Ploog, Phys. Rev. Lett. **68**, 1371 (1992).

[16] E. B. Foxman, P. L. McEuen, U. Meirav, N. S. Wingreen, Y. Meir, P. A. Belk, N. R. Belk, M. A. Kastner, and S. J. Wind, Phys. Rev. B **47**, 10 020 (1993).

[17] G. W. Bryant, Phys. Rev. Lett. **59**, 1140 (1987).

[18] A. Kumar, S. E. Laux, and F. Stern, Phys. Rev. B **42**, 5166 (1990).

[19] P. A. Maksym and T. Chakraborty, Phys. Rev. Lett. **65**, 108 (1990).

[20] U. Merkt, J. Huser, and M. Wagner, Phys. Rev. B **43**, 7320 (1991).

[21] Y. Meir, N. S. Wingreen, and P. A. Lee, Phys. Rev. Lett. **66**, 3048 (1991).

[22] C. W. J. Beenakker, Phys. Rev. B **44**, 1646 (1991).

[23] C. W. J. Beenakker, H. van Houten, and A. A. M. Staring, Phys. Rev. B **44**, 1657 (1991).

[24] N. F. Johnson and M. C. Paine, Phys. Rev. B **45**, 3819 (1992).

[25] R. A. Jalabert, D. A. Stone, and Y. Alhassid, Phys. Rev. Lett. **68**, 3468 (1992).

[26] J. J. Palacios, L. Martin-Moreno, and C. Tejedor, Physica B **189**, 27 (1993).

[27] J. J. Palacios and C. Tejedor, Phys. Rev. B **48**, 5386 (1993).

[28] K. Vacek, A. Okiji, and H. Kasai, Technol. Rep. Osaka Univ. **42**, 225 (1992).

[29] R. J. Brown, C. D. Smith, M. Pepper, M. J. Kelly, R. Newbury, H. Ahmed, D. G. Hasko, J. E. F. Forst, D. C. Peacock, D. A. Ritchie, and G. A. C. Jones, J. Phys. Condens. Matter **1**, 6291 (1989).

[30] H. Tamura and T. Ando, Phys. Rev. B **44**, 1792 (1991).

[31] R. L. Schult, H. W. Wyld, and D. G. Ravenhall, Phys. Rev. B **41**, 12 760 (1990).

[32] K.-F. Berggren and Zhen-Li Ji, Phys. Rev. B **43**, 4760 (1991).

[33] S. Chaudhuri, S. Bandyopadhyay, and M. Cahay, Phys. Rev. B **47**, 12 649 (1993).

[34] Hua Wu, D. W. L. Sprung, J. Martorell, and S. Klarsfeld, Phys. Rev. B **44**, 6351 (1991).
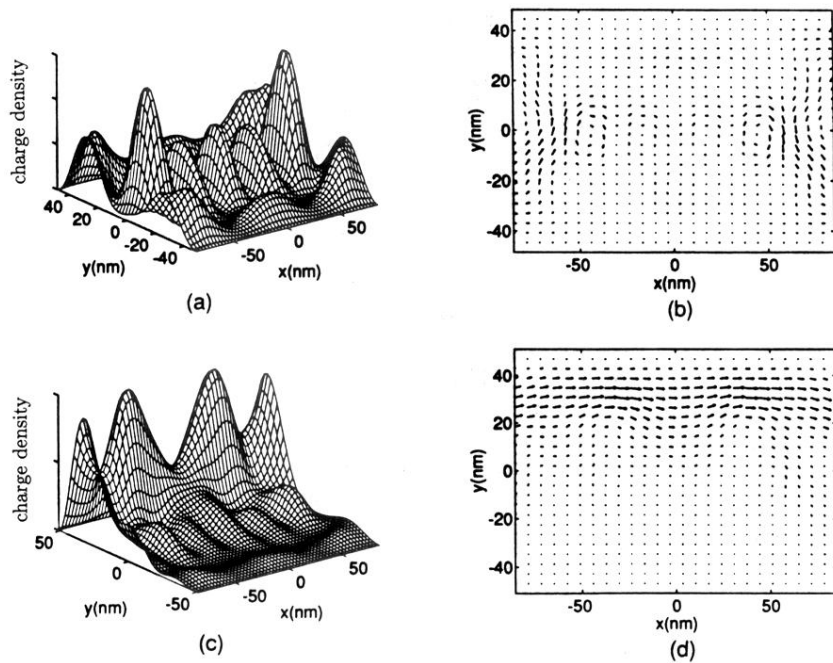
FIG. 6. The spatial distributions for the cases denoted by the arrows in Fig. 5. (a) The charge-density distribution associated with the resonant tunneling via a 0D state at $W = 96.9$ nm, denoted by a solid arrow in Fig. 5. (b) The current distribution associated with the charge-density distribution in (a). (c) The charge-density distribution at $W = 101.5$ nm, denoted by a dotted arrow also in Fig. 5. (d) The current distribution associated with the charge-density distribution in (c). The bulk of the forward current is carried by edge states.